

Analytic PCA Construction for Theoretical Analysis of Lighting Variability in Images of a Lambertian Object

Ravi Ramamoorthi

Abstract—We analyze theoretically the subspace best approximating images of a convex Lambertian object taken from the same viewpoint, but under different distant illumination conditions. Since the lighting is an arbitrary function, the space of all possible images is formally infinite-dimensional. However, previous empirical work has shown that images of largely diffuse objects actually lie very close to a five-dimensional subspace. In this paper, we analytically construct the principal component analysis for images of a convex Lambertian object, explicitly taking attached shadows into account, and find the principal eigenmodes and eigenvalues with respect to lighting variability. Our analysis makes use of an analytic formula for the irradiance in terms of spherical-harmonic coefficients of the illumination and shows, under appropriate assumptions, that the principal components or eigenvectors are identical to the spherical harmonic basis functions evaluated at the surface normal vectors. Our main contribution is in extending these results to the single-viewpoint case, showing how the principal eigenmodes and eigenvalues are affected when only a limited subset (the upper hemisphere) of normals is available and the spherical harmonics are no longer orthonormal over the restricted domain. Our results are very close, both qualitatively and quantitatively, to previous empirical observations and represent the first essentially complete theoretical explanation of these observations. Our analysis is also likely to be of interest in other areas of computer vision and image-based rendering. In particular, our results indicate that using complex illumination for photometric problems in computer vision is not significantly more difficult than using directional sources.

Index Terms—Illumination, radiance, irradiance, Lambertian, recognition, principal component analysis, spherical harmonics.

1 INTRODUCTION

A robust recognition system must be able to identify an object across variable lighting conditions. This is often a challenging task. For instance, it has been shown empirically by Moses et al. [13] that, in images of a human face, variability due to illumination changes is greater than that owing to differences between individual faces. Furthermore, most supposedly “illumination-invariant” features, such as edge maps, are, in practice, not robust to large lighting variations [13]. For this reason, it is important to come up with a low-dimensional generative model to explain lighting variability.

A classic approach to constructing such a representation is to consider the principal components of a set of images acquired under different conditions. This method is also sometimes called a Karhunen-Loeve expansion. This so-called *eigenface* approach has been described by Kirby and Sirovich [9], Sirovich and Kirby [20], and Turk and Pentland [21]. Often, we can achieve a good low-dimensional representation of the space of possible images by considering only a few principal components or eigenvectors—the modes corresponding to the largest eigenvalues.

With respect to lighting variability, however, the space of possible images is infinite-dimensional. Theoretical work by Bellhumeur and Kriegman [3] has shown that this is true even

for Lambertian objects under distant illumination—a common assumption made in many computer vision applications that we will make in this paper. Indeed, to represent the illumination exactly, we need an infinite number of coefficients, corresponding to the intensity for each incident direction. It would appear that each illumination condition leads to a distinct appearance for the object under consideration, making it impossible to derive a good low-dimensional subspace approximation using PCA.

However, experimental results go against this intuition. Empirical work is reported by Hallinan [8], Epstein et al. [5], and Yuille et al. [22]. They used a human face and other objects to perform PCA on a number of different images acquired by moving a distant point source along a sphere surrounding the object. These classic experiments came to the somewhat counterintuitive conclusion that, for largely diffuse objects, the first five principal components explain most of the image variation. In other words, images of diffuse objects under varying illumination lie very close to a 5D subspace.

Although the experiments by Hallinan [8] and Epstein et al. [5] are nearly a decade old, and have been confirmed by other authors [3], [6], [7], [22], there has been no satisfactory theoretical explanation. The closest prior work ignores the question of visibility, deriving the result that, in the absence of shadows, a 3D subspace suffices to describe the set of images of a Lambertian object under distant illumination [14], [18]. However, the absence of shadows is not a valid assumption in most practical situations. In reality, each point on an object is illuminated only from the upper hemisphere of incident directions. Attached shadows, referring to surface normals that face backward with respect to the light source and are therefore shadowed, are usually an important factor,

• The author is with the Department of Computer Science, Columbia University, 1214 Amsterdam Avenue, M.C. 0401, New York, NY 10027. E-mail: ravir@cs.columbia.edu.

Manuscript received 4 Oct. 2001; revised 16 Feb. 2002; accepted 19 Feb. 2002. Recommended for acceptance by P. Bellhumeur.

For information on obtaining reprints of this article, please send e-mail to: tpami@computer.org, and reference IEEECS Log Number 115140.

especially when the illumination is complex. For this reason, the 3D subspace approximations are too simple to explain the empirical data (which lies close to a 5D subspace).

Most recently, Basri and Jacobs [1] and Ramamoorthi and Hanrahan [16] have independently derived an analytic formula for the irradiance (and, hence, reflected radiance from a convex Lambertian object) under arbitrary distant illumination, explicitly considering attached shadows. They show that the irradiance can be regarded as a *convolution* of the incident illumination with the Lambertian reflectance function (*a clamped cosine*) and express the irradiance in terms of spherical harmonic coefficients of the illumination. A key result of their work is that Lambertian reflection acts as a low-pass filter so that the irradiance lies very close to a 9D subspace. This model is a significant step toward explaining why images of a diffuse object lie close to a low-dimensional subspace and provides novel frequency-space tools to understand lighting variability. However, the connection between the spherical harmonic basis and the principal components is not obvious. More importantly, the 9D subspace predicted is somewhat at variance with the 5D subspace observed empirically.

Given these discrepancies between previous analytical predictions and empirical observations, it appears that a complete theoretical explanation must explicitly construct the PCA. However, numerical PCA methods for empirical data sets usually operate on a small discrete set of images and may be biased by the particular lighting directions used. On the other hand, an analytical approach must consider an infinite set of images that correctly samples all possible illumination conditions. Furthermore, using a very dense discrete sampling of the sphere of incident illumination directions, with thousands of source images, would make PCA computationally intractable. For this reason, previous empirical work has not usually reported using very dense samplings nor has theoretical work tried a brute-force numerical computation of the PCA for synthetic images. However, there has recently been progress in analytically-based methods [10], [23] for extending PCA from a discrete set of images to a continuous sampling, with practical results demonstrating much better generalization than with a purely empirical method. In fact, Zhao and Yang [23] have analytically constructed the covariance matrix for PCA under the assumption of no shadowing.

In this paper, we analytically construct the PCA in terms of spherical harmonic basis functions, explicitly taking attached shadows into account, for images of a convex¹ Lambertian object under varying illumination, but fixed viewing conditions. In so doing, we uncover the connections between the spherical harmonic basis and the PCA. We show that, under appropriate assumptions, the principal components or eigenvectors are equal to the spherical harmonic basis functions and the eigenvalues, corresponding to how important a principal component is in explaining image variability, are equal to the spherical harmonic coefficients describing the Lambertian BRDF.

1. In other words, we explicitly take into account local attached shadows, i.e., normals back facing with respect to the illumination, but ignore the effects of global cast shadows. Hence, our method is not completely accurate for concave objects. However, as seen in the results, the agreement with experiment is excellent even when the surfaces have a few concave regions, such as human faces.

Next, we extend these results even further. Our main contribution is in showing how the eigenvectors (principal components) and eigenvalues are affected by restricting attention to a single viewpoint—where we have only the upper hemisphere of normals, instead of the whole sphere of surface orientations. While it is clear qualitatively that restricting the space of surface normals should produce a lower-dimensional approximation, this paper is the first disciplined approach to taking this restriction into account. In particular, we show that the reduced dimensionality stems from the fact that, while the spherical harmonics are orthonormal over the entire sphere of normals, this no longer holds over a reduced domain. This requires us to linearly combine the spherical harmonics to create a new set of orthonormal eigenfunctions over the reduced domain. The eigenvalue spectrum also changes, with a faster decay of eigenvalues, and a breaking of some of the degeneracies present when considering the entire sphere of surface normals. We show that one can numerically compute the eigenvectors and eigenvalues to very high accuracy simply by computing the eigensystem of a 9×9 matrix, making use of the 9D approximation introduced by Basri and Jacobs [1] and Ramamoorthi and Hanrahan [16].

Besides being of theoretical interest, this analysis gives analytic forms for the modified lighting and appearance basis functions to be used in object recognition. In this way, we extend the nine parameter Lambertian BRDF model, showing how to modify it when we have only a single viewpoint. Furthermore, the results point to a way of extending other computer vision algorithms to handle complex illumination. Our theoretical predictions, summarized below, are seen to be very close both qualitatively and quantitatively, to the previous empirical observations of Hallinan [8] and Epstein et al. [5].

Orthogonality Matrix. The major mathematical result is that the principal components and associated eigenvalues correspond to the eigenvectors of a scaled version of the *orthogonality matrix*, i.e., a matrix expressing the orthogonality between the spherical harmonic basis functions when the domain of integration is restricted to the surface normals in the image. If we were considering the entire sphere of possible normal directions, this matrix would just be the identity matrix. Hence, the eigenvectors or principal components would simply be the spherical harmonic modes. However, if we consider images from a single viewpoint, the orthogonality matrix is no longer the identity and the eigenvectors or principal components are linear combinations of the spherical harmonics, with a new eigenvalue spectrum. The orthogonality matrix depends on the distribution of surface normals in the image and, hence, depends on object geometry. We are able to derive quantitative results for a number of cases of interest, including images of a human face and a sphere, shown in Figs. 1 and 2, respectively.

Form of Principal Components: Hallinan [8] characterizes the first five principal components for human faces as corresponding to *frontal lighting*, *side lighting*, *lighting from above/below*, *extreme side lighting*, and *lighting from a corner*. Visual inspection of Figs. 1 and 2 indicates that the principal components predicted by our theoretical model agree well

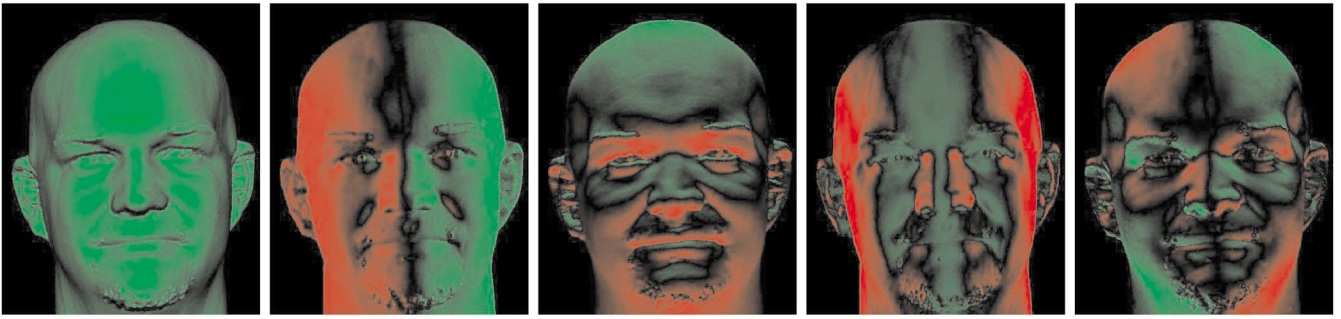


Fig. 1. The first five principal components of a face, computed by our method. The form of these eigenmodes is strikingly similar to those derived empirically by previous researchers (see Fig. 1 in Hallinan [8]). The corresponding eigenvalues are in the ratio of 0.42, 0.33, 0.16, 0.035, 0.021 and are in agreement with empirical observation, with the first five eigenmodes accounting for 97 percent of the variance. The principal components contain both positive values, shown in green, and negative values, shown in red. The face is an actual range scan courtesy of Cyberware.

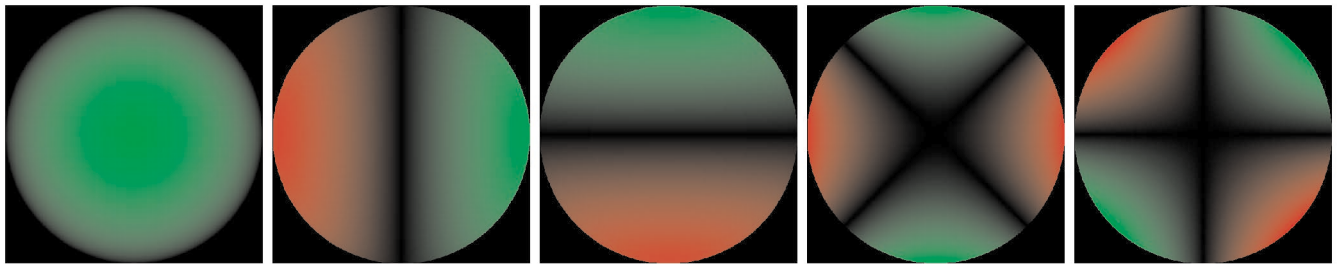


Fig. 2. The first five principal components for an image of a sphere, as computed analytically by our method. The corresponding eigenvalues are in the ratio of 0.43, 0.24, 0.24, 0.023, 0.023, with the first five eigenvalues accounting for 96 percent of the variance. The principal components contain both positive values, shown in green, and the negative values, shown in red.

with these labelings. Furthermore, Fig. 1 looks almost identical to Fig. 1 in Hallinan [8].²

Dimensionality of Approximating Linear Subspace.

From our derivation, we conclude that five eigenvectors or principal components suffice to capture over 95 percent of the image variance. These results agree with empirical work [8], [5]. In fact, we even have good quantitative agreement. For instance, Epstein et al. [5] report that, for an image of a basketball, three eigenvectors capture 94 percent of the variance, while five eigenvectors account for 98 percent. Our corresponding theoretical results for an image of a sphere are 91 percent and 96 percent. For a human face, the corresponding empirical numbers [5] for three and five eigenvectors are 90 percent and 94 percent, respectively. Our corresponding theoretical predictions are 91 percent and 97 percent, respectively.

Eigenvalue Spectrum. Hallinan [8] notes that, for human faces, the principal components lie in two groups. In a group, the eigenvalues are similar so the principal components may exchange places. The first group, consisting of two members, corresponds to frontal and side lighting. This is in agreement with our theoretical predictions, illustrated in Fig. 1, which show these two eigenvalues to be close, having numerical values 0.42 and 0.33 respectively, and well separated from

the other eigenvalues. The next group consists of the next three principal components. Our theory predicts that the eigenvalues for the fourth and fifth principal components are close (having values 0.035 and 0.021), so these may exchange places, as observed by Hallinan [8]. We predict that the third principal component should always correspond approximately to lighting from above/below, i.e., the Y direction. This appears to be the case in the empirical data also.

The rest of this paper is organized as follows: In Section 2, we mathematically show how to analytically construct the PCA, deriving the result that the principal components correspond to eigenvectors of the scaled orthogonality matrix. In Section 3, we use these results to actually compute the eigensystem, i.e., principal components and eigenvalues, for several cases of interest. In Section 4, we redo the computations with the mean value subtracted, as is conventional in PCA. The results of this section can directly be compared to experiment. Finally, Section 5 concludes the paper by presenting implications for a number of areas in computer vision and graphics, as well as suggesting some directions for future work. This paper is an expanded and more detailed version of the work [15] presented at the CVPR2001 workshop on identifying objects across lighting variations.

2 MATHEMATICS OF ANALYTIC PCA CONSTRUCTION

In this section, we give the mathematical details of our approach to analytic PCA construction. We first define the notation and the appropriate matrices. We then show how to reduce the problem to an eigensystem. In the next section, we will compute the eigenmodes for a number of cases of interest. There are two points worth noting about

2. We would like to propose a correction to his terminology, however. Eigenvectors 4 and 5 involve second order or quadratic modes and, therefore, cannot really be simply classified as corresponding to a single source of illumination. In fact, all the eigenmodes except the first have negative lobes as well as positive and cannot therefore be thought of as corresponding to any physical illumination. Hence, we think it should be emphasized that the principal components do not necessarily correspond to physical lighting conditions since they may take negative values. It may be more appropriate in the future to label the eigenvectors based on how they correspond to the spherical harmonic basis functions.

the mathematics. First, our original derivation will be without subtracting out the mean, as opposed to the common practice in PCA analysis. This will make the derivation slightly simpler and confer some interesting insights. Later, we will redo the analysis with the mean subtracted in order to make a more accurate comparison to empirical work. Second, we assume untextured surfaces. This assumption does not significantly affect the validity of our results since we may simply multiply all the principal components by the same texture in order to obtain results for textured objects. However, it should be noted that consideration of texture causes the principal components to have greater amplitude in regions of high albedo. For objects of interest for us, such as human faces, this effect is unlikely to be significant since the low-frequency texture variations are relatively minor.

2.1 Principal Component Analysis

We first define the notation. We will be interested in images $E(\alpha, \beta)$ corresponding to a light source at direction (α, β) , where (α, β) are the global spherical coordinates of the distant light source. A single pixel in the image will be denoted by $E(\alpha, \beta, \theta, \phi)$, where (θ, ϕ) stand for the spherical coordinates of the surface normal. Note that, in our model of the world (distant illumination, convex Lambertian surfaces, no cast shadows), these four parameters suffice to determine the shading. Also, since the surface is Lambertian and we are ignoring the albedo, $E(\alpha, \beta, \theta, \phi)$ can be thought of as corresponding directly to the irradiance at orientation (θ, ϕ) due to a unit directional source at (α, β) .

Assume now that we sample the space of possible image pixels in some way, i.e., by means of some light source positions $(\alpha_\rho, \beta_\rho)$ and some normal coordinates, i.e., (θ_i, ϕ_i) . The matrix Q consisting of all observations then has the form

$$Q_{i\rho} = E(\alpha_\rho, \beta_\rho, \theta_i, \phi_i). \quad (1)$$

Here, the rows (depending on index i) denote image observations, while the columns (depending on index ρ) correspond to different light source positions. This is the standard definition of the matrix Q . In order to find the principal components or eigenimages, we must find the eigensystem of the matrix $T = QQ^T$. The formula for this matrix is given by

$$\begin{aligned} T_{ij} &= \sum_{\rho} Q_{i\rho} Q_{\rho j}^T = \sum_{\rho} Q_{i\rho} Q_{\rho j} \\ &= \sum_{\rho} E(\alpha_\rho, \beta_\rho, \theta_i, \phi_i) E(\alpha_\rho, \beta_\rho, \theta_j, \phi_j). \end{aligned} \quad (2)$$

To help make matters concrete, assume that, in an experimental situation, there are n image pixels and d light positions. In most experiments, $n > d$. Then, matrix Q will be $n \times d$, while matrix T will be $n \times n$. The eigenvectors of T will correspond to principal component images, while the eigenvalues will measure their importance. We can get an idea of how well the matrix T is approximated by some number of eigenvectors by considering the fraction of the total sum of eigenvalues given by the sum of the eigenvalues corresponding to the eigenvectors in question. It should be noted that, in practical applications, it is possible to write down an equivalent $d \times d$ eigensystem that is computationally simpler. However, for analytic PCA construction, we work directly with the matrix T .

To proceed further, we will need a formula for E . We make use of a frequency-space analytic formula for the irradiance derived independently by Ramamoorthi and Hanrahan [16] as well as Basri and Jacobs [1].

$$E(\alpha, \beta, \theta, \phi) = \sum_{l=0}^{\infty} \sum_{m=-l}^l \hat{A}_l L_{lm}(\alpha, \beta) Y_{lm}(\theta, \phi). \quad (3)$$

In (3) above, Y_{lm} are the spherical harmonics [4], [11], [19]. Spherical harmonics with $l \geq 0$ and $-l \leq m \leq l$ are the appropriate signal processing tools in angular space and are the spherical analog of the conventional Fourier basis. The coefficients L_{lm} are the spherical harmonic coefficients of the incident illumination, while \hat{A}_l is a constant which vanishes for odd $l > 1$ and decays for even l as $l^{-5/2}$. Because of this rapid decay, a very good approximation can be obtained by limiting $l \leq 2$. In fact, 99 percent of the energy of the Lambertian BRDF filter, i.e., of \hat{A}_l , is contained by $l \leq 2$. Appendix A lists values for \hat{A}_l and Y_{lm} for $l \leq 2$.

The above formula describes the effects of general illumination conditions. We must specialize it to our case of a single-directional source by finding the coefficients $L_{lm}(\alpha, \beta)$ in terms of the angular coordinates (α, β) of the light source. Since the light source is described by a delta function, we simply evaluate the spherical harmonics at the light vector, deriving $L_{lm}(\alpha, \beta) = Y_{lm}(\alpha, \beta)$. Note that we use the real form of the spherical harmonics, so there is no need to worry about complex conjugation. Now,

$$E(\alpha, \beta, \theta, \phi) = \sum_{l=0}^{\infty} \sum_{m=-l}^l \hat{A}_l Y_{lm}(\alpha, \beta) Y_{lm}(\theta, \phi). \quad (4)$$

It is worthwhile contrasting (4) with the standard angular-space formula for E , obtained simply by the dot product of the vectors corresponding to (α, β) and (θ, ϕ) .

$$E(\alpha, \beta, \theta, \phi) = \max[0, \sin \alpha \sin \theta \cos(\beta - \phi) + \cos \alpha \cos \theta]. \quad (5)$$

The angular-space formula above is difficult to manipulate because of the max expression. The main advantage of the frequency-space formula in (4) is that no special case manipulation is required to treat attached shadows.

Plugging (4) into (2), we get

$$\begin{aligned} T_{ij} &= \sum_{l,m,l',m'} \hat{A}_l \hat{A}_{l'} Y_{lm}(\theta_i, \phi_i) Y_{l'm'}(\theta_j, \phi_j) \\ &\quad \times \sum_{\rho} Y_{lm}(\alpha_\rho, \beta_\rho) Y_{l'm'}(\alpha_\rho, \beta_\rho). \end{aligned} \quad (6)$$

We now proceed to do the summation over ρ . Clearly, this will depend, in practice, on the specific sampling pattern used for moving the light source. However, our goal is to get an analytic understanding. It is most reasonable to assume, for mathematical purposes, that the light source samples are infinitely dense, sampling the sphere of directions equally for all differential solid angles. This assumption also makes physical sense since we wish to make no a priori assumptions about the lighting distribution in the scene, so we should assume the illumination is equally likely to come from any direction. The summation over the index ρ may then be replaced by an integral over the angular coordinates (α, β) , and we obtain

$$T_{ij} = \sum_{l,m,l',m'} \hat{A}_l \hat{A}_{l'} Y_{lm}(\theta_i, \phi_i) Y_{l'm'}(\theta_j, \phi_j) \times \int_{\alpha=0}^{\pi} \int_{\beta=0}^{2\pi} Y_{lm}(\alpha, \beta) Y_{l'm'}(\alpha, \beta) \sin \alpha \, d\alpha \, d\beta. \quad (7)$$

It is now straightforward to use the orthonormality of the spherical harmonics to set $l = l'$ and $m = m'$ and write

$$T_{ij} = \sum_{l=0}^{\infty} \sum_{m=-l}^l \left(\hat{A}_l \right)^2 Y_{lm}(\theta_i, \phi_i) Y_{lm}(\theta_j, \phi_j). \quad (8)$$

We have just derived an analytic form for the elements T_{ij} of the covariance matrix used for principal component analysis. This analytic form has been derived under fairly weak assumptions—a convex Lambertian surface under distant illumination, with a uniform probability for the lighting over the entire sphere of incident directions. We now show how to derive the corresponding eigensystem.

2.2 Reduction to Eigensystem

We now wish to find an eigenvector u , which is a vector that satisfies $Tu = \lambda u$, where λ is the eigenvalue. This can also be written as $\sum_j T_{ij} u_j = \lambda u_i$. Note that u corresponds to a principal component image. Now, we expand u in terms of spherical harmonics,

$$u_j = \sum_{p=0}^{\infty} \sum_{q=-p}^p c_{pq} Y_{pq}(\theta_j, \phi_j). \quad (9)$$

Our goal is to find the coefficients c_{pq} . Plugging into (8), we obtain

$$\sum_j T_{ij} u_j = \sum_{l,m,p,q,j} \left(\hat{A}_l \right)^2 Y_{lm}(\theta_i, \phi_i) Y_{lm}(\theta_j, \phi_j) c_{pq} Y_{pq}(\theta_j, \phi_j) \quad (10)$$

$$\lambda u_i = \lambda \sum_{l,m} c_{lm} Y_{lm}(\theta_i, \phi_i).$$

We require the first and second lines above to be equal. First, we do the summation over the index j in the first line above. Define

$$M_{lm;pq} = \sum_j Y_{lm}(\theta_j, \phi_j) Y_{pq}(\theta_j, \phi_j). \quad (11)$$

The matrix M will be fundamental in the ensuing discussion. It indicates how orthogonal the various spherical harmonics are when the domain of integration is taken as the pixels of the image. In the special case where image pixels correspond uniformly to the entire sphere of surface normals, the orthonormality relation for the spherical harmonics will hold and the matrix M will simply be the identity with $M_{lm;pq} = \delta_{lp} \delta_{mq}$. However, this condition is never satisfied in practice since we never see the normals facing away from us. Later, in the next section, we will consider various matrices M and determine the resulting eigenmodes.

In terms of the matrix M , it is straightforward to write

$$\sum_j T_{ij} u_j = \sum_{l,m,p,q} \left(\hat{A}_l \right)^2 M_{lm;pq} c_{pq} Y_{lm}(\theta_i, \phi_i). \quad (12)$$

This expression may be compared to the first line of (10). The right-hand side must therefore equal the right-hand side in the second line. Since the spherical harmonics are linearly

independent, the coefficients of the Y_{lm} must match and we obtain

$$\sum_{p,q} \left(\hat{A}_l \right)^2 M_{lm;pq} c_{pq} = \lambda c_{lm}. \quad (13)$$

Thus, we have reduced the problem of computing the principal components to an eigenvalue problem involving the matrix M , which may be thought of as the frequency-space analog of the standard covariance matrix.

To proceed further, we will make a number of notational changes. First, let us collapse the double indices lm and pq into a single index in the standard way, i.e., $r = l^2 + l + m$ and $s = p^2 + p + q$. r and s simply impose an absolute ordering on the spherical harmonics, first on the index l or p and then on m or q . Next, we define $\hat{A}_r = \hat{A}_l$, i.e., we use the value of l corresponding to that value of r . To make things more concrete, consider Y_{21} in double-index form. Here, $l = 2$, $m = 1$, and $r = 7$. Hence, the spherical harmonic would be written Y_7 in single-index notation. In double-index notation, we would use \hat{A}_2 for all the Y_{2m} . In single-index notation, we use the same numerical value, but now denote it as \hat{A}_7 . Refer to Appendix A for mathematical values of the spherical harmonics and constants \hat{A} in both single and double index notation. Finally, define $\hat{M}_{rs} = \left(\hat{A}_r \right)^2 M_{rs}$, where $\hat{A}_r = \hat{A}_l$. It should be noted that, while the matrix M is symmetric, the matrix \hat{M} is no longer symmetric because of the premultiplication factor. It is now straightforward to write (13) as

$$\sum_s \hat{M}_{rs} c_s = \lambda c_r. \quad (14)$$

But, this is simply an eigenvalue problem with $\hat{M}c = \lambda c$. Thus, we have reduced the principal component analysis problem to an eigenvalue problem for \hat{M} . However, remember that the matrix \hat{M} is no longer symmetric. It often helps to work with symmetric matrices since their eigensystems have a number of nice properties. It is straightforward to rescale the matrices and vectors for symmetry. We first define a new symmetric matrix \tilde{M} and vector d by

$$c_r = \hat{A}_r d_r \quad (15)$$

$$\tilde{M}_{rs} = \hat{A}_r \hat{A}_s M_{rs}.$$

Now, starting with the basic matrix eigensystem in (14), we make the following substitutions:

$$\sum_s \hat{A}_r \hat{A}_s M_{rs} c_s = \lambda c_r$$

$$\Rightarrow \sum_s \hat{A}_r \left(\hat{A}_r M_{rs} \hat{A}_s \right) d_s = \lambda \hat{A}_r d_r \quad (16)$$

$$\Rightarrow \tilde{M} d = \lambda d.$$

Thus, we now have a symmetric eigensystem that can be solved for the vectors d . To find the eigenvectors of the original problem, we must find the corresponding vectors c using (15). The eigenvalues remain the same.

3 COMPUTATION OF EIGENMODES

Our goals now are to actually compute the eigenvectors and eigenvalues for various different values of the matrix \tilde{M} . However, this matrix is infinite dimensional since both r and s

can be arbitrarily large, corresponding to all possible spherical harmonic coefficients. Thus, it would appear that we are no better off in the frequency domain than using a brute force numerical technique in the angular domain. However, our analysis in terms of spherical harmonics allows for principled approximations to be made that make actual computation tractable. Specifically, it has been shown [1], [16] that 99 percent of the energy of the Lambertian BRDF is captured by $l \leq 2$, i.e., by $r, s < 9$. In other words, only the first nine spherical harmonic terms are important and there is little error introduced by truncating the series to order 2. Therefore, for numerical calculations in the rest of this section, we will use the nine term approximation, reducing matrix \tilde{M} to a 9×9 matrix. To verify the accuracy of this approximation, we will also compare one of our results to the eigensystem computed using a much larger value of $l \leq 6$, i.e., $r, s < 49$. We analyze the resulting eigensystem for many choices of the matrix \tilde{M} . It should be emphasized that the analytic formulas we derive are general and hold for all values of r and s . It is only the computed numerical values of the eigenvectors and eigenvalues that depend on the nine term (or higher) approximation.

Now, we find the principal components for several special cases of interest by considering the corresponding values of \tilde{M} and computing the eigensystem. We first explicitly write down the formula for M by rewriting (11) as per our modified notation:

$$\tilde{M}_{rs} = \hat{A}_r \hat{A}_s \sum_j Y_r(\theta_j, \phi_j) Y_s(\theta_j, \phi_j). \quad (17)$$

3.1 Pixels Equally Distributed over Sphere

The first special case of interest is when the pixels j are distributed in such a way that the sum can be replaced with an integral over the entire sphere. As already mentioned, this is unrealistic, but is nevertheless an insightful special case. In that case, orthonormality of the spherical harmonics yields

$$\begin{aligned} \tilde{M}_{rs} &= \hat{A}_r \hat{A}_s \int_{\theta=0}^{\pi} \int_{\phi=0}^{2\pi} Y_r(\theta, \phi) Y_s(\theta, \phi) \sin \theta d\theta d\phi \\ &= \hat{A}_r \hat{A}_s \delta_{rs} = (\hat{A}_r)^2 \delta_{rs}. \end{aligned} \quad (18)$$

In other words, \tilde{M} is a diagonal matrix. The eigenvectors or principal components (for both d and c) are simply the spherical harmonics themselves with eigenvalues $(\hat{A}_r)^2$. The amount of variance accounted for by some number of eigenvectors is simply the sum of the corresponding eigenvalues divided by the sum of all the eigenvalues. This corresponds to the case previously studied by Basri and Jacobs [1] and Ramamoorthi and Hanrahan [16]. As noted by Basri and Jacobs [1], 37.5 percent of the variance is accounted for by the constant term $l = 0; r, s < 1$, 87.5 percent of the variance is accounted for when also considering the linear terms $l \leq 1; r, s < 4$, and over 99 percent of the variance is accounted for when considering the quadratic terms, i.e., all nine terms in our approximation: $l \leq 2; r, s < 9$. Thus, we see that our formulation agrees with the previous subspace results. It is worth pointing out an important special case or corollary here. Shashua [18] has considered the situation

where there are no attached shadows. In this case, the images of a Lambertian object lie exactly in a three-dimensional subspace. We can consider this case in our formulation by removing the threshold to 0 in our definition of the Lambertian BRDF intensity of (5). In terms of the above formulation, \hat{A}_r would vanish unless $l = 1$ (the linear terms), i.e., $r = 1, 2, 3$. Thus, the eigenvectors would be exactly the linear spherical harmonics and, as noted by Shashua [18], a 3D subspace would suffice.

3.2 Pixels Equally Distributed over Hemisphere

We now consider a more realistic case. Since only front facing normals are visible in a single image, we allow the pixels to be equally distributed over the hemisphere with $z > 0$. In the standard spherical coordinates, this corresponds to $\theta < \pi/2$. The matrix M now encodes how orthogonal the spherical harmonics are when the domain of integration is restricted to the upper hemisphere. While linear independence of the spherical harmonics guarantees that no linear combination can have norm 0, we will see that the norm of certain linear combinations comes very close to 0, i.e., most of the norm is concentrated over the unseen lower hemisphere. Thus, these lighting configurations have negligible impact on the irradiance of the upper hemisphere and may be neglected.

It is now straightforward to define

$$\tilde{M}_{rs} = \hat{A}_r \hat{A}_s \int_{\theta=0}^{\pi/2} \int_{\phi=0}^{2\pi} Y_r(\theta, \phi) Y_s(\theta, \phi) \sin \theta d\theta d\phi. \quad (19)$$

It should be noted that $\tilde{M}_{rs} \neq 0$ only for terms having the same m index, i.e., those with $m = 0$: Y_0, Y_2, Y_6 (corresponding in two-index notation to Y_{00}, Y_{10}, Y_{20}), those with $m = -1$: Y_1, Y_5 (corresponding to Y_{1-1} and Y_{2-1}), and those with $m = 1$: Y_3, Y_7 (corresponding to Y_{11} and Y_{21}). We have not included $m = \pm 2$ since there is only one term with that value of m (Y_4, Y_8 corresponding to Y_{2-2} and Y_{22} , respectively). All other cross terms will vanish. Also, cross terms involving odd ($l + m$ odd) and even ($l + m$ even) spherical harmonics only vanish. Hence, the cross terms between Y_0 and Y_6 vanish. Thus, the effects of rearranging the integration to lie over the hemisphere rather than the full sphere will be the intermingling of the basis functions corresponding to $m = 0$ and those corresponding to $m = 1$ and $m = -1$. Y_4 and Y_8 , corresponding to $m = \pm 2$, will remain eigenvectors of \tilde{M} and are not affected by this intermingling.

It is now straightforward to compute the matrix \tilde{M} and its eigensystem. We used Mathematica for this purpose. The diagonal terms of \tilde{M} are as follows: The factor of π^2 comes from the formulas for \hat{A} and the factor of $1/2$ from the integration being done over the hemisphere rather than the sphere. The terms below are simply $\frac{1}{2}(\hat{A}_r)^2$.

$$\begin{aligned} \tilde{M}_{00}/\pi^2 &= \frac{1}{2} \\ \tilde{M}_{11}/\pi^2 &= \tilde{M}_{22}/\pi^2 = \tilde{M}_{33}/\pi^2 = \frac{2}{9} \\ \tilde{M}_{44}/\pi^2 &= \tilde{M}_{55}/\pi^2 = \tilde{M}_{66}/\pi^2 = \tilde{M}_{77}/\pi^2 = \tilde{M}_{88}/\pi^2 = \frac{1}{32}. \end{aligned} \quad (20)$$

The nonzero off-diagonal terms are as follows (we show only terms with $r \leq s$ since \tilde{M} is symmetric):

$$\begin{aligned}\tilde{M}_{02}/\pi^2 &= \frac{1}{2\sqrt{3}} \\ \tilde{M}_{15}/\pi^2 &= \frac{\sqrt{5}}{32} \\ \tilde{M}_{26}/\pi^2 &= \frac{1}{32}\sqrt{\frac{5}{3}} \\ \tilde{M}_{37}/\pi^2 &= \frac{\sqrt{5}}{32}.\end{aligned}\quad (21)$$

The eigensystem of the matrix can now be found analytically, but the results are complicated and do not confer any special insights. Instead, we give, in Table 1, the numerical forms for the eigenvectors and eigenvalues. The eigenvectors are normalized to have unit norm and are determined only up to sign. The eigenvalues are normalized to be the percentage of the total sum of the nine eigenvalues. They thus correspond to the fraction of variance accounted for by that particular eigenvector. We also show the cumulative sum of eigenvalues. This indicates how well the image is approximated using only a number of the most important principal components. To account for components not considered by us, i.e., terms higher than order 2, we multiply the eigenvalues by 0.99, corresponding to the amount of energy captured by the first nine terms, i.e., modes up to order 2. It should be noted that this is only an approximation. However, exact bounds on the nine term error for any physical lighting distribution can be derived from the fact that the lighting must be everywhere positive, using an approach similar to that of Basri and Jacobs [1].

The four columns in Table 1 stand for the eigenvectors d of the matrix \tilde{M} , the corresponding eigenvectors c of the original PCA (as per (15))—note that these have more energy in the lower frequencies—the normalized eigenvalues λ , and the cumulative sum of eigenvalues, corresponding to the variance accounted for (VAF).

Note that the eigenvectors split into groups corresponding to the value of m , i.e., the azimuthal dependence. Thus, there are three eigenvectors (those numbered 1, 4, 9) composed of linear combinations of Y_0, Y_2, Y_6 . This group of eigenvectors has no azimuthal dependence ($m = 0$). There are other groups with $m = 1$ (eigenvectors 2 and 7 involving Y_3 and Y_7), and $m = -1$ (eigenvectors 3 and 8 involving Y_1 and Y_5). In all of these cases, restriction to the hemisphere instead of the sphere causes us to obtain *mixed eigenvectors*, where basis functions that would be orthogonal over the entire sphere combine. Finally, we have the eigenvectors Y_4 and Y_8 corresponding to $m = -2$ and $m = 2$, respectively, which are not mixed and not affected by restriction to the hemisphere.

Another noteworthy point is that 98 percent of the variance is accounted for using only the first six principal components or eigenvectors. The observation that fewer than nine eigenvectors suffice for an accurate approximation is not really surprising. Intuitively, over the visible hemisphere where $z > 0$, the basis functions y and yz or x and xz (corresponding, respectively, to Y_1 and Y_5 or Y_3 and Y_7) are very similar. Furthermore, one can show from first principles that there must be at least one eigenvector with a negligible eigenvalue. Our numerical calculations are based

TABLE 1
Eigenvectors and Eigenvalues for the Hemisphere

#	Eigenvector d	Eigenvector c	λ	VAF
1	.85 Y_0 + .53 Y_2 + .03 Y_6	.92 Y_0 + .39 Y_2 + .01 Y_6	.51	.51
2	.95 Y_3 + .31 Y_7	.99 Y_3 + .12 Y_7	.18	.69
3	.95 Y_1 + .31 Y_5	.99 Y_1 + .12 Y_5	.18	.88
4	-.42 Y_0 + .63 Y_2 + .65 Y_6	-.68 Y_0 + .68 Y_2 + .26 Y_6	.05	.93
5	Y_8	Y_8	.023	.95
6	Y_4	Y_4	.023	.98
7	-.31 Y_3 + .95 Y_7	-.66 Y_3 + .75 Y_7	.006	.98
8	-.31 Y_1 + .95 Y_5	-.66 Y_1 + .75 Y_5	.006	.99
9	.32 Y_0 - .57 Y_2 + .76 Y_6	.61 Y_0 - .71 Y_2 + .35 Y_6	.0008	.99

on the observation that the *half-cosine* function can be well-approximated using spherical harmonics up to order 2, which allows us to use the 9×9 matrix approximation for numerical work. But, this also means that the *backward half-cosine function*, which has its positive lobe in the lower hemisphere and is zero over the visible upper hemisphere, is well-approximated using spherical harmonics up to order 2. This approximation has negligible norm over the visible upper hemisphere.

To formalize this observation, note that the *backward half-cosine function* can be written as $\max[0, -\cos\theta]$. This function is positive when $\theta \in [\frac{\pi}{2}, \pi]$ in the lower hemisphere and is 0 over the upper hemisphere $[0, \frac{\pi}{2}]$. Now, consider the representation of this function using spherical harmonics up to order 2. Straightforward integration to find coefficients yields

$$\begin{aligned}\max[0, -\cos\theta] &\approx \frac{\sqrt{\pi}}{2} Y_0 - \sqrt{\frac{\pi}{3}} Y_2 + \frac{\sqrt{5\pi}}{8} Y_6 \\ &= 0.89Y_0 - 1.02Y_2 + 0.50Y_6.\end{aligned}\quad (22)$$

This is simply the spherical harmonic representation of the cosine function, and an analytic formula for arbitrary orders can be derived [1], [16]. Upon renormalizing and rescaling, we obtain

$$0.694 \max[0, -\cos\theta] \approx 0.61Y_0 - 0.71Y_2 + 0.35Y_6. \quad (23)$$

Indeed, we see that the right-hand side corresponds directly to the ninth eigenvector c in Table 1, i.e., the ninth principal component is the normalized *backward half-cosine*, with the corresponding eigenvalue being nearly three orders of magnitude smaller than the largest eigenvalue.

Finally, we verify the accuracy of our computation using the 9×9 matrix approximation. To do so, we go through the same calculation, but using matrices to order 6 instead of order 2, i.e., 49×49 instead³ of 9×9 . This order 6 approximation captures 99.92 percent of the energy of the Lambertian BRDF filter, as opposed to 99.2 percent with an order 2 (nine term) approximation. The results in Table 2 are almost identical to those in Table 1, showing the correctness of the calculation using the 9D approximation.

3. It can be shown [1], [16] that the contributions due to odd order harmonics greater than order one vanish. Hence, there are really only 31 relevant terms and a 31×31 matrix would suffice.

TABLE 2

The First Nine Eigenvectors and Eigenvalues for the Hemisphere Using an Order 6, i.e., 49×49 Matrix

#	Eigenvector d	Eigenvector c	λ	VAF
1	$.85 Y_0 + .53 Y_2 + .03 Y_6$	$.92 Y_0 + .39 Y_2 + .01 Y_6$.51	.51
2	$.95 Y_3 + .31 Y_7$	$.99 Y_3 + .12 Y_7$.18	.70
3	$.95 Y_1 + .31 Y_5$	$.99 Y_1 + .12 Y_5$.18	.88
4	$-.42 Y_0 + .63 Y_2 + .65 Y_6$	$-.68 Y_0 + .68 Y_2 + .26 Y_6$.05	.93
5	Y_8	Y_8	.023	.96
6	Y_4	Y_4	.023	.98
7	$-.30 Y_3 + .93 Y_7$	$-.65 Y_3 + .75 Y_7$.0065	.986
8	$-.30 Y_1 + .93 Y_5$	$-.65 Y_1 + .75 Y_5$.0065	.993
9	$.25 Y_0 - .43 Y_2 + .58 Y_6 - .64 Y_{20}$	$.61 Y_0 - .70 Y_2 + .35 Y_6 - .07 Y_{20}$.0014	.994

We note that the first nine eigenmodes in Table 2 account for 99.4 percent of the variance, justifying our multiplying the variance accounted for by 0.99 in Table 1 to account for the 9D approximation. The only nontrivial difference in Table 2 is the slightly different form of the ninth eigenvector. This now includes a significant contribution from the spherical harmonic Y_{20} in single index form, i.e., the fourth-order harmonic Y_{40} in double index form, and the eigenvalue is also appreciably higher. Since the *backward half-cosine* has such a low norm over the visible hemisphere, it is reasonable that a more accurate computation of the ninth eigenvector includes higher-order terms, which increase the eigenvalue somewhat. In fact, the coefficient of the fourth order term is the negative of what it would be in the fourth order approximation of the *backward half-cosine* function.

3.3 Image of a Sphere

While the previous section gave considerable insight, it does not correspond to a realistic situation. This is because, in practice, the number of pixels occupied by regions at oblique angles to the camera is reduced by a cosine factor when projected down into the camera plane. Thus, we should consider that factor when doing the integrations. Hence, we add a factor of $\cos \theta$ in (19):

$$\tilde{M}_{rs} = \hat{A}_r \hat{A}_s \int_{\theta=0}^{\pi/2} \int_{\phi=0}^{2\pi} Y_r(\theta, \phi) Y_s(\theta, \phi) \cos \theta \sin \theta d\theta d\phi. \quad (24)$$

Note that this does not change the azimuthal structure of the matrix M . Thus, our previous discussion regarding the groups for the eigenvectors for different values m continues to hold. The diagonal terms in the matrix \tilde{M} now are

$$\begin{aligned} \tilde{M}_{00}/\pi^2 &= \frac{1}{4} \\ \tilde{M}_{11}/\pi^2 &= \tilde{M}_{33}/\pi^2 = \frac{1}{12} \\ \tilde{M}_{22}/\pi^2 &= \frac{1}{6} \\ \tilde{M}_{44}/\pi^2 &= \tilde{M}_{88}/\pi^2 = \frac{5}{512} \\ \tilde{M}_{55}/\pi^2 &= \tilde{M}_{66}/\pi^2 = \tilde{M}_{77}/\pi^2 = \frac{5}{256}. \end{aligned} \quad (25)$$

TABLE 3

Eigenvectors and Eigenvalues for Image of a Sphere

#	Eigenvector d	Eigenvector c	λ	VAF
1	$.77 Y_0 + .63 Y_2 + .14 Y_6$	$.88 Y_0 + .48 Y_2 + .04 Y_6$.62	.62
2	$.91 Y_3 + .42 Y_7$	$.99 Y_3 + .17 Y_7$.15	.77
3	$.91 Y_1 + .42 Y_5$	$.99 Y_1 + .17 Y_5$.15	.92
4	$-.52 Y_0 + .48 Y_2 + .71 Y_6$	$-.82 Y_0 + .51 Y_2 + .28 Y_6$.034	.95
5	Y_4	Y_4	.015	.97
6	Y_8	Y_8	.015	.98
7	$-.42 Y_3 + .91 Y_7$	$-.78 Y_3 + .63 Y_7$.004	.99
8	$-.42 Y_1 + .91 Y_5$	$-.78 Y_1 + .63 Y_5$.004	.99
9	$.38 Y_0 - .62 Y_2 + .69 Y_6$	$.65 Y_0 - .70 Y_2 + .30 Y_6$.0004	.99

The nonzero off-diagonal terms are:

$$\begin{aligned} \tilde{M}_{02}/\pi^2 &= \frac{1}{3\sqrt{3}} \\ \tilde{M}_{06}/\pi^2 &= \frac{\sqrt{5}}{64} \\ \tilde{M}_{15}/\pi^2 &= \frac{1}{12\sqrt{5}} \\ \tilde{M}_{26}/\pi^2 &= \frac{1}{6\sqrt{15}} \\ \tilde{M}_{37}/\pi^2 &= \frac{1}{12\sqrt{5}}. \end{aligned} \quad (26)$$

Finally, the eigensystem is given in Table 3 and is largely similar to that in Table 1.

3.4 Image of a Face

To more accurately compare our predictions to those of Hallinan [8], we would ideally like to consider the image of a face rather than a sphere. Hence, we took a range scan of a face (courtesy of Cyberware) and raytraced a single frontal image, storing the surface normal, i.e., (θ, ϕ) at each pixel. Since we do not explicitly consider variation in surface texture, we ignored any albedo information in the input data. We could then evaluate the matrix \tilde{M} directly in a numerical fashion, using (17), by summing over all pixels. While the azimuthal structure is still nearly preserved, numerically, all elements of the matrix \tilde{M} will be nonzero, unlike in the previous sections. The eigenvectors and eigenvalues are listed in Table 4. These are quite similar to those in Table 3. It should be noted that the numerical values depend on the specific face model used by us and will differ slightly for other faces. As before, five or six principal components suffice to explain almost the entire sequence of images. In fact, three principal components predict 92 percent of the image, while five predict 97 percent. Perhaps the most important feature of the face geometry, that distinguishes it from an image of a sphere, is that the symmetry between side and top directions is now broken because of the asymmetric dimensions of the face. In fact, the eigenvalue corresponding to side lighting (#2) is almost twice as large as that for vertical lighting (#3).

TABLE 4
Eigenvectors and Eigenvalues for the Image of a Face

#	Eigenvector d	Eigenvector c	λ	VAF
1	$.77 Y_0 + .62 Y_2 + .12 Y_6$	$.88 Y_0 + .48 Y_2$.61	.61
2	$.91 Y_3 + .40 Y_7$	$.98 Y_3 + .16 Y_7$.21	.82
3	$-.10 Y_0 + .89 Y_1 + .44 Y_5$	$-.15 Y_0 + .97 Y_1 + .18 Y_5$.10	.92
4	$-.43 Y_0 + .46 Y_2 + .65 Y_6 - .41 Y_8$	$-.76 Y_0 + .54 Y_2 + .29 Y_6 - .18 Y_8$.038	.96
5	$-.06 Y_3 + .99 Y_4$	$-.15 Y_3 + .98 Y_4$.013	.97
6	$-.24 Y_0 + .16 Y_2 + .30 Y_6 + .90 Y_8$	$-.68 Y_0 + .30 Y_2 + .20 Y_6 + .63 Y_8$.010	.98
7	$-.40 Y_3 + .91 Y_7$	$-.75 Y_3 + .65 Y_7$.004	.99
8	$-.44 Y_1 + .89 Y_5$	$-.79 Y_1 + .60 Y_5$.002	.99
9	$.39 Y_0 - .62 Y_2 + .68 Y_6$	$.65 Y_0 - .70 Y_2 + .29 Y_6$.002	.99

For clarity and ease of comparison, only those spherical harmonics with nonnegligible coefficient magnitudes (greater than 0.10) are noted here.

4 RESULTS WITH REMOVAL OF MEAN VALUE

One final point in attempting a quantitative comparison with the work of Hallinan [8] and Epstein et al. [5] concerns removal of the mean value before taking the PCA. As is the standard practice when computing principal components, those authors have subtracted the mean value before applying their analysis. We have so far chosen not to do so because the mathematics is somewhat simpler to explain when retaining the mean value and we believe there are valuable insights in the previous section. Furthermore, in many applications, the numerical forms of the basis functions derived in the previous section are likely to be useful.

However, it is not significantly more difficult to apply our framework with the mean image value removed. In this section, we will extend our results under those conditions. It can be shown that removing the mean simply corresponds to ignoring the constant or ambient term Y_0 or Y_{00} . Alternatively, we may set $\hat{A}_0 = 0$. This makes intuitive sense since the ambient term simply sets the mean value. The same result can also be derived through some simple algebra on the definition of the PCA and is presented in Appendix B. We will now numerically use an 8×8 matrix and eight eigenvectors and eigenvalues since the mean term will no longer contribute.

We first show the eigenvectors and eigenvalues for the case of an image of a sphere with the constant term subtracted in Table 5.

The first three eigenmodes are now very clearly identifiable as frontal, side, and top/bottom lighting, while the next two are quadratic modes. Three eigenvectors account for 91 percent of the variance and five eigenvectors for 96 percent. These results clearly show why the first five eigenvectors form a stable group that is a good approximation in a variety of circumstances. Furthermore, our numerical values are quantitatively similar to the empirical results quoted by Epstein et al. [5] for an image of a basketball, wherein three eigenvectors captured 94 percent of the variance, while five eigenvectors accounted for 98 percent. The somewhat better low-dimensional fit obtained by Epstein et al. [5] can be at least partially explained by the details of their experiment. Their lighting conditions sampled only part of the illumination sphere (the top right), while we make the more general assumption of light sources equally sampling the entire sphere of incident directions. It should be noted that the sixth eigenvector, although having

TABLE 5
Eigenvectors and Eigenvalues for Image of the Sphere with the Mean Image Value Subtracted Out (i.e., Ignoring the Ambient Term)

#	Eigenvector d	Eigenvector c	λ	VAF
1	$.97 Y_2 + .26 Y_6$	$.99 Y_2 + .10 Y_6$.43	.43
2	$.91 Y_3 + .42 Y_7$	$.99 Y_3 + .17 Y_7$.24	.67
3	$.95 Y_1 + .31 Y_5$	$.99 Y_1 + .17 Y_5$.24	.91
4	Y_8	Y_8	.023	.94
5	Y_4	Y_4	.023	.96
6	$-.26 Y_2 + .97 Y_6$	$-.59 Y_2 + .81 Y_6$.019	.98
7	$-.42 Y_3 + .91 Y_7$	$-.78 Y_3 + .63 Y_7$.006	.98
8	$-.42 Y_1 + .91 Y_5$	$-.78 Y_1 + .63 Y_5$.006	.99

eigenvalue similar to eigenvectors 4 and 5, corresponds to a backlighting configuration not well sampled experimentally by Hallinan [8] and Epstein et al. [5].

Finally, we can look at the eigenvectors and values for an image of a face after the mean has been subtracted. As before, the eigenvectors are largely similar to those above, with the specific numerical values dependent on the specific face model used by us. However, it should be noted that there are some subtle differences between face and sphere eigenvectors, as can be seen by comparing eigenvector 4 (second from right) in Figs. 1 and 2 or Tables 5 and 6. The eigenvectors and eigenvalue spectrum are shown below in Table 6 as well as Fig. 3.

The significant difference compared to the sphere is that the eigenvalue for side lighting (eigenvalue #2) is substantially higher than that for top/bottom lighting (eigenvalue #3) and is in fact comparable to the eigenvalue for frontal lighting (eigenvalue #1). The spherical symmetry between side and top/bottom (X and Y) directions is broken since human faces are elongated and curve more sideways; they are not symmetric about X and Y directions as in a sphere.

TABLE 6
Eigenvectors and Eigenvalues for Image of a Face with the Mean Image Value Subtracted Out (i.e., Ignoring the Ambient Term)

#	Eigenvector d	Eigenvector c	λ	VAF
1	$.15 Y_1 + .95 Y_2 + .24 Y_6$	$.15 Y_1 + .98 Y_2 + .09 Y_6$.42	.42
2	$.91 Y_3 + .40 Y_7$	$.98 Y_3 + .16 Y_7$.33	.75
3	$.88 Y_1 - .17 Y_2 + .44 Y_5$	$.96 Y_1 - .19 Y_2 + .18 Y_5$.16	.91
4	$.09 Y_2 + .13 Y_4 - .58 Y_6 + .80 Y_8$	$.24 Y_2 + .12 Y_4 - .56 Y_6 + .77 Y_8$.035	.95
5	$-.06 Y_3 + .98 Y_4 - .14 Y_8$	$-.15 Y_3 + .97 Y_4 - .14 Y_8$.021	.97
6	$-.23 Y_2 + .77 Y_6 + .58 Y_8$	$-.53 Y_2 + .67 Y_6 + .50 Y_8$.011	.98
7	$-.40 Y_3 + .91 Y_7$	$-.75 Y_3 + .64 Y_7$.007	.99
8	$-.44 Y_1 + .89 Y_5$	$-.79 Y_1 + .60 Y_5$.003	.99

For clarity and ease of comparison, only those spherical harmonics with nonnegligible coefficient magnitudes (greater than 0.10) are noted here.

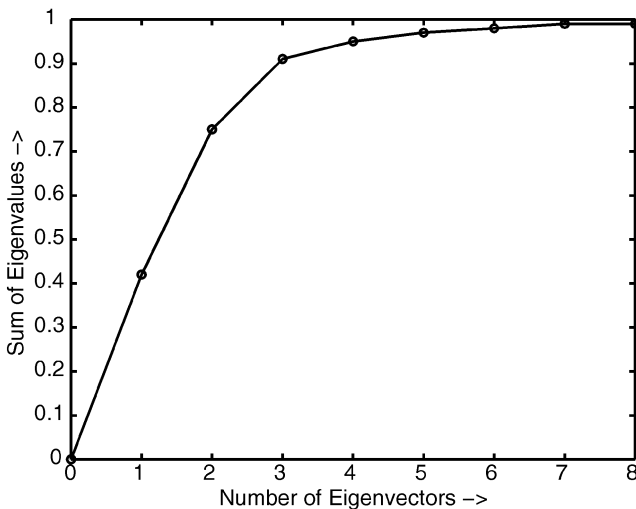


Fig. 3. Fraction of eigenvalues accounted for versus number of eigenvectors or principal components for PCA of a face with mean removed. Five principal components account for 97 percent of the variance.

These results explain Hallinan's observation that the eigenvectors split into two groups, with the first two eigenvectors corresponding to frontal and side lighting and the next three to top/bottom lighting and more extreme forms. It does appear from the eigenvalues in Table 6 that the eigenvector corresponding to top/bottom lighting should always appear in third position and the empirical data appear to confirm this. The quantitative predictions for variance accounted for are also in accordance with empirical work. The empirical numbers given by Epstein et al. [5] for the variance accounted for by three and five eigenvectors in images of a human face are 90 percent and 94 percent, respectively. Specularity and a small amount of cast-shadowing accounts for the slightly lower numbers as compared to the basketball example. Our corresponding theoretical predictions are 91 percent and 97 percent, respectively. These are slightly higher than the empirical values because we assume Lambertian surfaces and do not take cast shadows into account. Finally, Fig. 1 indicates that the principal components predicted by us are in very good agreement with those from Fig. 1 in Hallinan [8]. Also, the descriptions attached by Hallinan, namely ambient/frontal lighting, side, top/bottom, extreme side, and corner lighting are all consistent with the principal components predicted by our theory.

5 CONCLUSIONS AND FUTURE WORK

We have presented a method to analytically construct the principal components for images of a Lambertian object from a single viewpoint, under varying distant illumination, explicitly taking attached shadows into account. From this construction, we derive a number of results including good approximating low-dimensional subspaces, the forms of the principal components, and the eigenvalue spectra of the eigenmodes. These results show excellent qualitative and quantitative agreement with previous empirical work. Besides explaining a number of previous papers on lighting variability, the results are likely to be of considerable practical interest in a number of areas of computer vision and graphics.

- Identifying Objects across Lighting Variability.** With respect to both human and machine vision, our results indicate that lighting variability may not be that significant an obstacle to object recognition. Under the assumptions made by us, images from a single view-point always lie very close to a 5D subspace, regardless of the complexity of the illumination. From a practical point of view, we derive explicit forms for the principal components. The benefit of having these analytic basis functions has already been demonstrated by Basri and Jacobs [1] and Zhao and Yang [23]. From our analysis, it is clear that our basis functions are optimal for constructing principal component images. A subspace recognition method can then simply check if a new image lies in the subspace spanned by these principal components in order to determine if this is an image of a particular object under novel lighting conditions.
- Complex Illumination in Computer Vision.** In the past, essentially all photometric computer vision algorithms have been restricted to working under a single point or directional source or at most a combination of a small number of point sources. Further, many methods assume absence of shadowing, i.e., that all points are visible to all sources. However, lighting in most real indoor and outdoor scenes is complex, coming from a variety of point and area sources. Furthermore, in almost all situations, only a part of the incident illumination will be visible (i.e., front facing) for any surface point. The framework outlined in this paper provides a general approach for handling complex illumination while taking attached shadows into account. One of the key results of this paper is that complex illumination is not significantly more difficult to handle than point sources. We simply need to consider a few additional basis functions, i.e., 5D or 6D subspaces instead of 3D. The forms of the appropriate basis functions have also been analytically derived by us. One simply needs to project the complex incident illumination onto these basis functions, representing the lighting and irradiance by the coefficients in these projections. There are a number of problems in computer vision, such as photometric stereo, shape from shading, estimation of texture under complex lighting, and others, where we believe this approach will allow the use of general, complex illumination conditions.
- Inverse Rendering.** An area of growing importance in computer vision and graphics is *inverse rendering*—the determination of illumination and reflectance properties from images. In previous work, Ramamoorthi and Hanrahan [16], [17] have cast inverse rendering as a deconvolution algorithm and shown some fundamental limits to what information can be estimated. However, their analysis is based on having complete information about the entire 4D reflected light field, i.e., the exitant radiance for all surface normal orientations and all outgoing directions. In practice, when we have one or a small number of images, the

information available is significantly less. This paper is a first step in analyzing how having only part of the reflected light field available affects the well-posedness and conditioning of inverse problems. Specifically, our results show that, from a single image of a Lambertian object of known geometry, only the first five or six coefficients of the illumination can be reliably estimated. On the other hand, if multiple views, covering all surface normals are available, all of the first nine modes of the illumination—corresponding to spherical harmonics of order 0,1, and 2—can be estimated [16].

- **Image-Based Rendering.** Given views of a diffuse object under a few lighting conditions, we may form the basis images for the illumination modes corresponding to the principal components. These can then be efficiently combined to obtain new images for arbitrary illumination conditions. Conceptually, this method is similar to that of Malzbender et al. [12]. However, by analytically constructing the PCA, we can determine the appropriate choice of basis functions instead of selecting them in an ad hoc manner. Furthermore, our approach allows the use of complex illumination instead of directional sources; we can express any illumination condition (and the resulting image) as a linear combination of basis functions.

In future work, we would like to extend our derivation to consider nonuniform sampling patterns for the light source, corresponding to preferred directions of illumination. Slightly better quantitative agreement with experiment might also be obtained by considering a higher-dimensional approximation than the 9×9 orthogonality matrix we use for numerical work here and by explicitly accounting for variation in surface albedos. We would also like to incorporate specularly in our analysis. From a practical point of view, we would like to implement some of the algorithms proposed here for problems such as photometric stereo, inverse rendering, and image-based rendering. In this connection, it is worth noting that Basri and Jacobs [2] have already considered photometric stereo under unknown general lighting.

Finally, we note that this paper has developed a significantly new set of tools for analyzing lighting variability and for analytically constructing principal components. We expect these and more advanced methods to be of increasing significance in principal component analysis, object recognition, and other areas of computer vision.

APPENDIX A

SPHERICAL HARMONICS

Below, we list the values of the constants \hat{A} as well as the real forms of the first nine spherical harmonics, used for computation, in both single and double index form.

In double-index notation, such as in (3) and (4), the constants \hat{A}_l , corresponding to the spherical harmonic Y_{lm} are given by

$$\hat{A}_0 = \pi \quad \hat{A}_1 = 2\pi/3 \quad \hat{A}_2 = \pi/4. \quad (27)$$

In single-index notation, such as in (15) and (16), the constants \hat{A} , corresponding to the spherical harmonics Y_r , are determined by the value of l corresponding to the single-index value of r , i.e.,

$$\begin{aligned} \hat{A}_0 &= \pi : l = 0 \\ \hat{A}_1, \hat{A}_2, \hat{A}_3 &= 2\pi/3 : l = 1 \\ \hat{A}_4, \hat{A}_5, \hat{A}_6, \hat{A}_7, \hat{A}_8 &= \pi/4 : l = 2. \end{aligned} \quad (28)$$

The spherical harmonics are simply constant, linear, and quadratic polynomials of the Cartesian components of the surface normal. However, it will be convenient here to write them in trigonometric form.

$$\begin{aligned} Y_0 &= Y_{00}(\theta, \phi) = \sqrt{\frac{1}{4\pi}} \\ Y_1 &= Y_{1-1}(\theta, \phi) = \sqrt{\frac{3}{4\pi}} \sin \theta \sin \phi \\ Y_2 &= Y_{10}(\theta, \phi) = \sqrt{\frac{3}{4\pi}} \cos \theta \\ Y_3 &= Y_{11}(\theta, \phi) = \sqrt{\frac{3}{4\pi}} \sin \theta \cos \phi \\ Y_4 &= Y_{2-2}(\theta, \phi) = \sqrt{\frac{15}{4\pi}} \sin^2 \theta \cos \phi \sin \phi \\ Y_5 &= Y_{2-1}(\theta, \phi) = \sqrt{\frac{15}{4\pi}} \sin \theta \cos \theta \sin \phi \\ Y_6 &= Y_{20}(\theta, \phi) = \sqrt{\frac{5}{16\pi}} (3 \cos^2 \theta - 1) \\ Y_7 &= Y_{21}(\theta, \phi) = \sqrt{\frac{15}{4\pi}} \sin \theta \cos \theta \cos \phi \\ Y_8 &= Y_{22}(\theta, \phi) = \sqrt{\frac{15}{16\pi}} (\sin^2 \theta (\cos^2 \phi - \sin^2 \phi)). \end{aligned} \quad (29)$$

APPENDIX B

MATHEMATICS OF PCA WITH MEAN REMOVED

The traditional approach to PCA construction is to subtract out the mean value, averaging over all pixels in all images. Effectively, this means that, instead of considering the irradiance E , we must consider $\tilde{E} = E - \mu$, where μ is a constant denoting the mean irradiance value. Making this substitution in (2), we obtain

$$\begin{aligned} \tilde{T}_{ij} &= \sum_{\rho} [E(\alpha_{\rho}, \beta_{\rho}, \theta_i, \phi_i) - \mu] [E(\alpha_{\rho}, \beta_{\rho}, \theta_j, \phi_j) - \mu] \\ &= T_{ij} - \mu \sum_{\rho} [E(\alpha_{\rho}, \beta_{\rho}, \theta_i, \phi_i) + E(\alpha_{\rho}, \beta_{\rho}, \theta_j, \phi_j)] + \sum_{\rho} \mu^2. \end{aligned} \quad (30)$$

It is simple to simplify this expression. Let $\gamma = \sum_{\rho} 1$, i.e., the number of images taken with different light source positions. Since we are assuming images equally sampling the sphere of possible light source directions, γ is just a measure of the solid angle subtended by a sphere and is therefore equal to 4π . Further note that, for any pixel orientation, the average value μ is just the average of E over all light source positions. This is because all light source directions are equally sampled; hence, the average intensity over all light source directions is the same regardless of pixel

orientation. Therefore, (30) simplifies upon grouping terms appropriately and substituting (8) to

$$\begin{aligned}\tilde{T}_{ij} &= T_{ij} - \mu \cdot 2\gamma\mu + \gamma\mu^2 \\ &= T_{ij} - \gamma\mu^2 \\ &= \left(\sum_{l=0}^{\infty} \sum_{m=-l}^l (\hat{A}_l)^2 Y_{lm}(\theta_i, \phi_i) Y_{lm}(\theta_j, \phi_j) \right) - \gamma\mu^2 \\ &= \left((\hat{A}_0 Y_{00})^2 - \gamma\mu^2 \right) \\ &\quad + \sum_{l=1}^{\infty} \sum_{m=-l}^l (\hat{A}_l)^2 Y_{lm}(\theta_i, \phi_i) Y_{lm}(\theta_j, \phi_j).\end{aligned}\quad (31)$$

Now, note that $(Y_{00})^2 = \frac{1}{4\pi}$. We can multiply and divide $\gamma\mu^2$ by this value to obtain

$$\begin{aligned}\tilde{T}_{ij} &= \left((\hat{A}_0)^2 - 4\pi\gamma\mu^2 \right) Y_{00}(\theta_i, \phi_i) Y_{00}(\theta_j, \phi_j) \\ &\quad + \sum_{l=1}^{\infty} \sum_{m=-l}^l (\hat{A}_l)^2 Y_{lm}(\theta_i, \phi_i) Y_{lm}(\theta_j, \phi_j).\end{aligned}\quad (32)$$

It is clear from this equation that subtracting out the mean in PCA construction is equivalent to replacing

$$\hat{A}_0 \rightarrow \sqrt{(\hat{A}_0)^2 - 4\pi\gamma\mu^2}.\quad (33)$$

Now, it is simply a question of substituting numerical values. We know that $\hat{A}_0 = \pi$ and $\gamma = 4\pi$. μ is the average irradiance, i.e., the average of $\max(\cos \theta, 0)$. Thus,

$$\mu = \frac{1}{4\pi} \int_{\theta=0}^{\pi/2} \int_{\phi=0}^{2\pi} \cos \theta \sin \theta \, d\theta \, d\phi = \frac{1}{4}.\quad (34)$$

Finally, making numerical substitutions in (33), we obtain

$$\hat{A}_0 \rightarrow \sqrt{\pi^2 - 4\pi \cdot 4\pi \cdot \left(\frac{1}{4}\right)^2} = 0.\quad (35)$$

ACKNOWLEDGMENTS

The author is grateful to Pat Hanrahan, Steve Marschner, and the anonymous reviewers for reading early drafts of this manuscript and providing many helpful suggestions. The work described in this paper was supported in part by a Hodgson-Reed Stanford graduate fellowship and US National Science Foundation (NSF) ITR grant #0085864 "Interacting with the Visual World."

REFERENCES

- [1] R. Basri and D. Jacobs, "Lambertian Reflectance and Linear Subspaces," *Proc. Eighth IEEE Int'l Conf. Computer Vision*, pp. 383-390, 2001.
- [2] R. Basri and D. Jacobs, "Photometric Stereo with General, Unknown Lighting," *Proc. Computer Vision and Pattern Recognition Conf.*, pp. II-374-II-381, 2001.
- [3] P. Belhumeur and D. Kriegman, "What Is the Set of Images of an Object under All Possible Illumination Conditions?" *Int'l J. Computer Vision*, vol. 28, no. 3, pp. 245-260, 1998.
- [4] B. Cabral, N. Max, and R. Springmeyer, "Bidirectional Reflection Functions from Surface Bump Maps," *Proc. ACM SIGGRAPH Conf.*, pp. 273-281, 1987.

- [5] R. Epstein, P. Hallinan, and A. Yuille, "5 Plus or Minus 2 Eigenimages Suffice: An Empirical Investigation of Low-Dimensional Lighting Models," *Proc. IEEE Workshop Physics-Based Modeling in Computer Vision*, pp. 108-116, 1995.
- [6] A. Georghiades, P. Belhumeur, and D. Kriegman, "From Few to Many: Generative Models for Recognition under Variable Pose and Illumination," *Proc. Fourth Int'l Conf. Automatic Face and Gesture Recognition*, pp. 277-284, 2000.
- [7] A. Georghiades, D. Kriegman, and P. Belhumeur, "Illumination Cones for Recognition under Variable Lighting: Faces," *Proc. Computer Vision and Pattern Recognition Conf.*, pp. 52-59, 1998.
- [8] P. Hallinan, "A Low-Dimensional Representation of Human Faces for Arbitrary Lighting Conditions," *Proc. Computer Vision and Pattern Recognition Conf.*, pp. 995-999, 1994.
- [9] M. Kirby and L. Sirovich, "Application of the Karhunen-Loeve Procedure for the Characterization of Human Faces," *IEEE Trans. Pattern Recognition and Machine Intelligence*, vol. 12, no. 1, pp. 103-108, Jan. 1990.
- [10] A. Levin and A. Shashua, "Principal Component Analysis over Continuous Subspaces and Intersection of Half-Spaces," *Proc. European Conf. Computer Vision*, to appear.
- [11] T.M. MacRobert, *Spherical Harmonics; An Elementary Treatise on Harmonic Functions, with Applications*. Dover Publications, 1948.
- [12] T. Malzbender, D. Gelb, and H. Wolters, "Polynomial Texture Maps," *Proc. ACM SIGGRAPH Conf.*, pp. 519-528, 2001.
- [13] Y. Moses, Y. Adini, and S. Ullman, "Face Recognition: The Problem of Compensating for Changes in Illumination Direction," *Proc. European Conf. Computer Vision*, pp. 286-296, 1994.
- [14] H. Murase and S. Nayar, "Visual Learning and Recognition of 3-D Objects from Appearance," *Int'l J. Computer Vision*, vol. 14, no. 1, pp. 5-24, 1995.
- [15] R. Ramamoorthi, "Analytic PCA Construction for Theoretical Analysis of Lighting Variability, Including Attached Shadows, in a Single Image of a Convex Lambertian Object," *Proc. Computer Vision and Pattern Recognition Conf. Workshop Identifying Objects across Variations in Lighting: Psychophysics and Computation*, pp. 48-55, 2001.
- [16] R. Ramamoorthi and P. Hanrahan, "On the Relationship between Radiance and Irradiance: Determining the Illumination from Images of a Convex Lambertian Object," *J. Optical Soc. Am. A*, vol. 18, no. 10, pp. 2448-2459, Oct. 2001.
- [17] R. Ramamoorthi and P. Hanrahan, "A Signal-Processing Framework for Inverse Rendering," *Proc. ACM SIGGRAPH Conf.*, pp. 117-128, 2001.
- [18] A. Shashua, "On Photometric Issues in 3D Visual Recognition from a Single 2D Image," *Int'l J. Computer Vision*, vol. 21, pp. 99-122, 1997.
- [19] F.X. Sillion, J. Arvo, S.H. Westin, and D. Greenberg, "A Global Illumination Solution for General Reflectance Distributions," *Proc. ACM SIGGRAPH Conf.*, pp. 187-196, 1991.
- [20] L. Sirovich and M. Kirby, "Low-Dimensional Procedure for the Characterization of Human Faces," *J. Optical Soc. Am. A (JOSA A)*, vol. 4, no. 3, pp. 519-524, Mar. 1987.
- [21] M. Turk and A. Pentland, "Eigenfaces for Recognition," *J. Cognitive Neuroscience*, vol. 3, no. 1, pp. 71-96, 1991.
- [22] A. Yuille, D. Snow, R. Epstein, and P. Belhumeur, "Determining Generative Models of Objects under Varying Illumination: Shape and Albedo from Multiple Images Using SVD and Integrability," *Int'l J. Computer Vision*, vol. 35, no. 3, pp. 203-222, 1999.
- [23] L. Zhao and Y. Yang, "Theoretical Analysis of Illumination in PCA-Based Vision Systems," *Pattern Recognition*, vol. 32, pp. 547-564, 1999.



Ravi Ramamoorthi received the BS in engineering and applied science and MS degrees in computer science and physics from the California Institute of Technology in 1998. He received his PhD degree in computer science from the Stanford University Computer Graphics Laboratory in 2002. He is currently an assistant professor of computer science at Columbia University. His research interests cover many topics in computer graphics and related areas of computer vision, including mathematical foundations, inverse modeling and rendering, efficient interactive rendering, object recognition, and optimal computer-generated animation. He has published papers on all of these topics in leading graphics and vision conferences and journals.